Applied Ocean Research 31 (2009) 143–156

Contents lists available at ScienceDirect

Applied Ocean Research

journal homepage: www.elsevier.com/locate/apor

Experimental investigation of water impact on axisymmetric bodies

G. De Backer [a,*], M. Vantorre [a], C. Beels [a], J. De Pré [a], S. Victor [a], J. De Rouck [a], C. Blommaert [b], W. Van Paepegem [b]

[a] Department of Civil Engineering, Ghent University, Technologiepark Zwijnaarde 904, B 9052 Zwijnaarde, Belgium
[b] Department of Materials Science and Engineering, Ghent University, Sint-Pietersnieuwstraat 41, B 9000 Gent, Belgium

ARTICLE INFO

Article history:
Received 31 October 2008
Received in revised form
27 April 2009
Accepted 15 July 2009
Available online 20 August 2009

Keywords:
Slamming
Drop tests
Point absorbers
Wave energy
Experimental study

ABSTRACT

The results of an elaborate experimental investigation on bottom slamming of axisymmetric objects are presented. Drop tests have been performed on a hemisphere and two conical shapes with different deadrise angles. The test setup is designed so as to prevent small rotations of the test objects which cause scatter in the measurement data. The pressure distribution and evolution as well as the body motion parameters are measured during impact. By means of a high speed camera the water uprise is visualized and the wetting factor is determined for the cones. The results are compared with a three-dimensional asymptotic theory for axisymmetric rigid bodies with constant entry velocity. The ratio between the registered peak pressures and the asymptotic theory are in accordance with comparable experiments in the literature. The asymptotic theory, however, is found to be quite conservative, since the measured peak pressure levels appear to be approximately 50% to 75% of the theoretical levels.

1. Introduction

An experimental test programme has been executed to investigate bottom slamming phenomena on point absorbers. Point absorber systems are wave energy converters consisting of oscillating bodies with horizontal dimensions that are small compared to the incident wavelength. Examples of point absorber devices are the FO^3 [1] and Wave Star Energy [2]. The point absorber buoys move according to one or more degrees of freedom (heave, surge, pitch, roll) as a response to incoming waves and their kinetic energy is transferred into electrical energy either directly or by means of a hydraulic intermediate stage. Since the buoys generally have a higher natural frequency than the dominant incident wave frequencies, the point absorber response is often tuned to the characteristics of the incoming wave spectrum by increasing the system inertia or by applying latching control [3]. This enables the point absorber to operate closer to resonance conditions, which increases the energy capture. However, it might cause the buoys to rise out of the water which results in slamming back into the water surface on re-entry. This phenomenon occurs particularly for point absorbers with a small draft in an energetic wave climate. Slamming can be reduced by influencing the control parameters of the buoy, i.e. by increasing the damping and/or by detuning the buoy. However, these measures result in power absorption losses as shown in [4,5]. Consequently, a certain level of slamming will usually be allowed. For this reason it is important to know to which pressure magnitudes the body is exposed when slamming occurs. This paper aims to investigate bottom slamming on point absorbers by means of experimental drop tests. The results are compared with analytical results obtained by Chuang [6] and Faltinsen and Zhao [7].

Slamming phenomena have been studied over several decades especially in naval hydrodynamics. Pioneering research has been carried out by von Karman [8] and Wagner [9]. Wagner studied the water impact on rigid two-dimensional bodies by approximating the bodies with a flat plate and taking into account the water uprise on the body in a simplified way. Because of the blunt body approach, the bodies are assumed to have small deadrise angles in the range of 4 up to 20 degrees [10]. Zhao and Faltinsen presented numerical results, based on the findings of Dobrovol'skaya [11], for two-dimensional bodies with deadrise angles between 4 and 81 degrees [12,13]. Inspired by Zhao's work, Mei et al. [14] developed an analytical solution for the water impact problem of general two-dimensional bodies. The main difference with the Wagner method is that the exact body boundary conditions are fulfilled, instead of approximating the body by a flat plate. The advantage of Wagner's approximation is the ability to use analytical expressions for the velocity potential. However, with the generalized Wagner method, a broader range of (local) deadrise angles can be investigated in a more accurate way.

* Corresponding author. Tel.: +32 9 264 54 93; fax: +32 9 264 58 37.
E-mail address: griet.debacker@ugent.be (G. De Backer).

0141-1187/$ – see front matter © 2009 Elsevier Ltd. All rights reserved.
doi:10.1016/j.apor.2009.07.003

Nomenclature

b_0	wet radius at the undisturbed free water surface [m]
b	wet radius at the immediate free water surface [m]
C_p	slamming pressure coefficient [-]
C_v	coefficient of variation [-]
C_w	wetting factor [-]
F	force [N]
g	gravitational acceleration [m/s^2]
h	drop height [m]
h^*	equivalent drop height corresponding to the measured impact velocity [m]
l_{jet}	jet height [m]
M	body mass [kg]
$M_{a_{33}}$	infinite frequency limit of the added mass [kg]
p	pressure [bar $= 10^5$ Pa]
r	radial coordinate [m]
R	radius of hemisphere [m]
$R*$	Pearson correlation coefficient [-]
t	time [s]
U	entry velocity [m/s]
z	vertical coordinate [m]
β	deadrise angle [deg][rad]
ζ	water elevation at intersection with body [m]
ρ	mass density of fluid [kg/m^3]

A substantial amount of experimental work has been performed to validate the analytical and numerical models. Lin and Shieh [15] experimentally investigated the pressure characteristics of a cylinder during water impact. They also visualized the flow pattern during penetration by making use of a digital imaging system and a high speed data acquisition system. Zhao and Faltinsen [13] performed drop tests to study two-dimensional flow situations of horizontal wedges dropped onto the free water surface. Experiments by Yettou [16] et al. consist of free fall drop tests on symmetrical wedges. They investigated the influence of the drop height, the deadrise angle and the mass of the wedge and compared the results with existing models from Mei et al. [14] and Zhao and Faltinsen [13].

Most studies have focused on two-dimensional impact problems since slamming on ships has been a major concern. However, there is a need for three-dimensional solutions because real impact phenomena are three dimensional. In this paper, vertical slamming of three-dimensional objects, more specific axisymmetric bodies, is considered. Early studies in this area have been published by Shiffman and Spencer [17,18]. They investigated vertical slamming phenomena on spheres and cones analytically by approximating the bodies as a lens and an ellipsoid and presented solutions for the impact force on these axisymmetric objects. Wagner's theory has been extended to axisymmetric bodies by Chuang [6] and Faltinsen and Zhao [7]. In the case of axisymmetric objects, the body shape is approximated with a growing flat disc analogous to Wagner's flat plate approximation for two-dimensional shapes. Based on this principle, Chuang [6] developed an analytical expression for the pressure distribution on a cone with small deadrise angle. In 1997 Faltinsen and Zhao [7] presented an asymptotic theory for water entry of hemispheres and cones with small (local) deadrise angles based on the assumptions behind the Wagner theory. Another important contributor to axisymmetric slamming problems is Miloh [19–21] who developed analytical expressions for the slamming forces on axisymmetric bodies. One of the main differences between his work and Wagner's theory is that the body boundary conditions are satisfied exactly on the actual body surface instead of on a flat disc.

In 2003 Battistin and Iafrati [22] numerically studied impact loads and pressure distributions on two-dimensional and axisymmetric bodies. Two years later Faltinsen and Chezhian [23] presented a generalized Wagner method for three-dimensional slamming based on the approach presented by Zhao et al. [13] for two-dimensional water impact problems. To validate the numerical simulations, they performed drop tests on a three-dimensional shiplike composite structure from which they obtained several force measurements. Peseux, Gornet and Donguy [24] solved the three-dimensional Wagner problem numerically for both rigid and deformable bodies. The numerical model is validated with an interesting experimental investigation consisting of drop tests of conical shapes with small deadrise angles ($6^\circ - 10^\circ - 14^\circ$). Kim and Hong [25] numerically studied the impact of arbitrary three-dimensional bodies with an extended von Karman and an extended Wagner approach, including the presence of incoming waves. They also presented experimental results on the impact loads during water entry of three-dimensional structures.

Very few experiments are available for validation of theoretical pressure predictions for axisymmetric bodies. In 1961 Nisewanger [26] performed drop tests on aluminium hemispheres and measured pressure distributions with self-made pressure transducers. For conical shapes, experimental research has been carried out by Chuang and Milne [27] in 1971 and more recently by Peseux et al. as mentioned above. In the former study impact pressures are measured on cone shapes with small deadrise angles varying from 1° to 15°. Point absorbers with a conical shape are very likely to have larger deadrise angles ($\geq 20^\circ$). In this paper the results of new impact experiments on a hemisphere and on cone shapes with larger deadrise angles are presented.

2. Experimental design

2.1. Test setup and test objects

Table 1 shows the three different bodies that have been tested: a hemisphere and two cones with deadrise angles of 20° and 45°. The models are made from polyurethane and have a large thickness from 30 mm to 50 mm. As mentioned in Table 1 the diameter of the objects is 0.30 m, which is sufficient to reduce surface tension effects. The bodies are dropped in a water basin with horizontal dimensions of 1.20 m by 1.00 m and a height of 1.25 m. Twelve different drop heights between 0.05 m and 2.00 m have been evaluated, corresponding to impact velocities of 1.0 m/s and 6.3 m/s. A realistic stroke for a point absorber buoy is about 5 to 10 m. Dependent on the control parameters, a free fall of 2 m can be considered as an extreme case. Smaller drop heights will occur more frequently and are therefore relevant as well. Because of reasons of similitude, the cone shape tests can be considered as full-scale tests, apart from the fact that the masses are not correctly scaled. In case of the hemisphere, the results from the smallest drop heights (0.05 m–0.20 m) need to be upscaled to prototype values, according to the dimensions of a full-scale body. Expected scaling effects might arise from surface tension and viscous effects. For completeness, the tests with the hemisphere are also performed for larger drop heights.

In this paper, the results of an improved test setup are presented. Initially the tests were carried out without any guiding structure. Although the test objects were balanced precisely, the scatter in the measured data appeared to be significant. In order to prevent small rotations of the floaters while falling down, the setup was equipped with a guiding system consisting of tightened steel wires [5]. The results discussed in this paper, however, are obtained from a test setup with an improved guiding system. The tightened steel rods are replaced by a rail mounted on stiff aluminium profiles. The test bodies are attached to a profile structure equipped

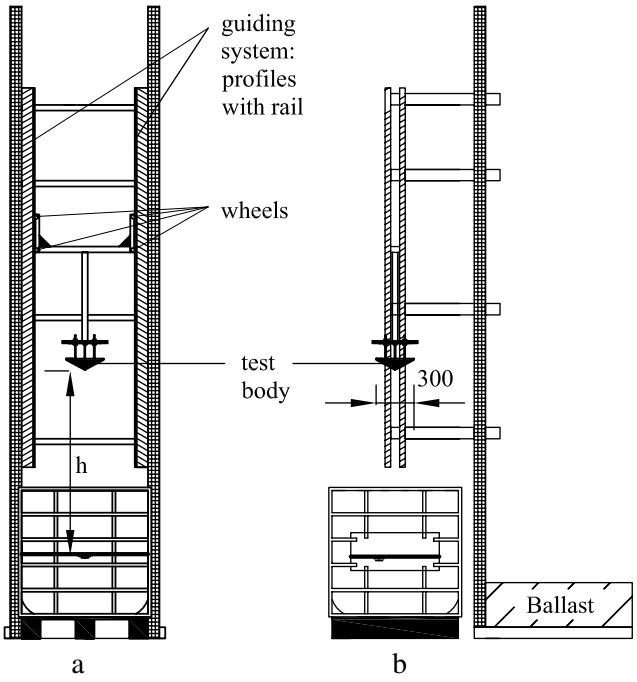

Fig. 1. Schematic view of the experimental test setup [mm].

Fig. 2. Picture of the experimental test setup.

with wheels, rolling down the rail as shown in Fig. 1. With this test setup the verticality of the impacting object is assured and the tests are very well reproducible. The masses mentioned in Table 1 correspond to the total falling mass, i.e. the sum of the mass of the polyurethane bodies and the aluminium carriage. The drop height, h, is limited to 2 m, compared to 4 m for the original test setup. A 10 mm plexiglass sheet is installed in the basin which allows to film the impact phenomena. A picture of the test setup is given in Fig. 2.

Table 1
Test object characteristics.

Test objects (dimensions in mm)	Characteristics
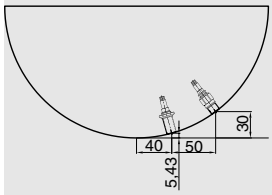	Hemisphere Local deadrise angles: 7.7° and 18.4° Radius: 0.15 m Material thickness: 0.05 m Mass: 11.5 kg
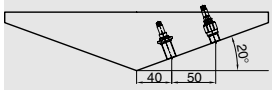	Cone Deadrise angle: 20° Max. radius: 0.15 m Material thickness: 0.03 m Mass: 9.8 kg
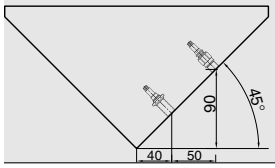	Cone Deadrise angle: 45° Max. radius: 0.15 m Material thickness: 0.03 m Mass: 10.2 kg

Table 2
Sensor characteristics.

Sensor	Measurement range	Resonance frequency (kHz)
A07	3.45 bar	≥ 250
K30, K31	2 bar	≥ 150
Shock accelerometer	500 g	≥ 54

2.2. Instrumentation

2.2.1. Pressure sensors and shock accelerometer

The pressure time history, the position and deceleration of the body were recorded during impact. Three high frequency piezoelectric pressure sensors were used. One ICP pressure sensor (A07) has a built-in microelectronic amplifier while two other high frequency pressure sensors (K30, K31) have external amplifiers. The measurement range for these devices is 3.45 bar and 2 bar, respectively. The pressure cells have a small diaphragm of 5.5 mm and a very high resonance frequency, see Table 2. Consequently the sensors are very well suited for measuring impact phenomena. The sensors are flush-mounted at a horizontal distance of 0.04 m and 0.09 m, respectively from the symmetry axis, as illustrated in Table 1. The deceleration of the object during impact was measured by a shock accelerometer with a measurement range up to 500 g and a resonance frequency of 54 kHz.

Fig. 3 shows the configuration of the pressure cells. The first three configurations (a–c) represent the sensor positions for the hemisphere. The sensors in Fig. 3(a) are mounted on two opposite meridians in order to evaluate the verticality of the penetration. With the configuration in Fig. 3(b) a comparison between the two local deadrise angles can be made and in Fig. 3(c) the sampling frequency is increased up to 100 kHz for one pressure sensor and the shock accelerometer. In Fig. 3(d) and (e) the configuration of the pressure sensors is given for the 20° cone. In each configuration two different pressure sensors are mounted on meridians close to each other, allowing for the assessment of the different sensors. Fig. 3(f) shows the pressure sensor configuration in case of the 45° cone, which is similar to Fig. 3(a) combined with (b). Each case has been tested at least three times for every drop height, varying between 0.05 m and 2 m.

A sampling frequency (SF) of at least 30 kHz was used for recording. Such high sampling frequencies are required, since the

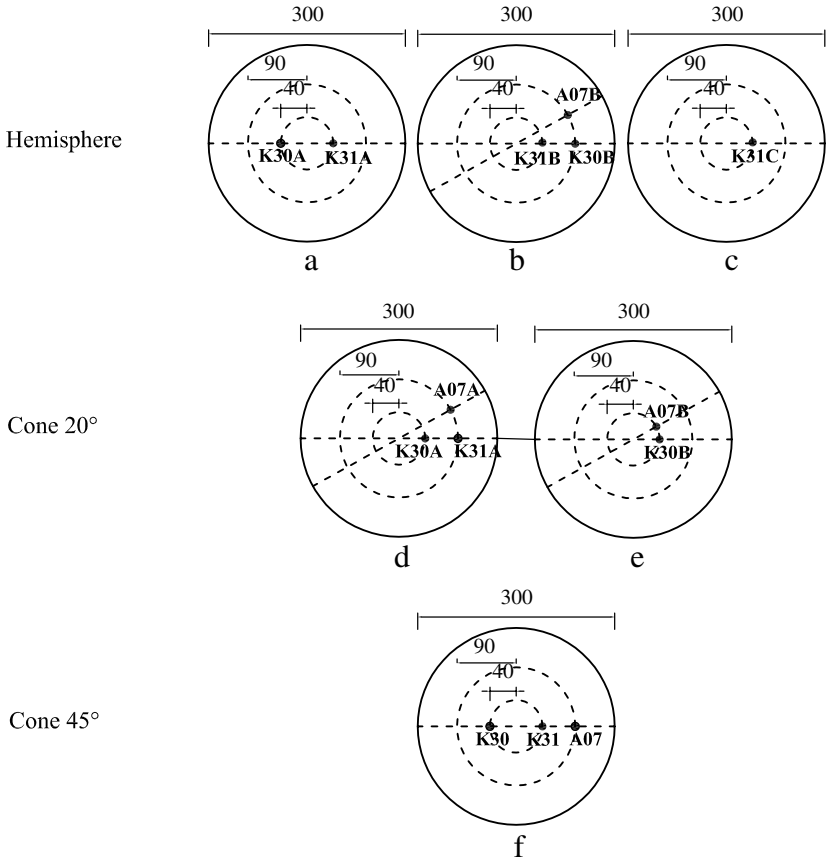

Fig. 3. Pressure sensor positions [mm] for the hemisphere: (a) Sensors K30A and K31A - SF = 30 kHz, (b) Sensors K30B, K31B and A07B - SF = 30 kHz, (c) Sensor K31C - SF = 100 kHz, for the 20° cone : (d) Sensors K30A, K31A and A07A - SF = 30 kHz, (e) Sensors K30B and A07B - SF = 30 kHz, for the 45° cone: (f) Sensors K30, K31 and A07 - SF = 30 kHz.

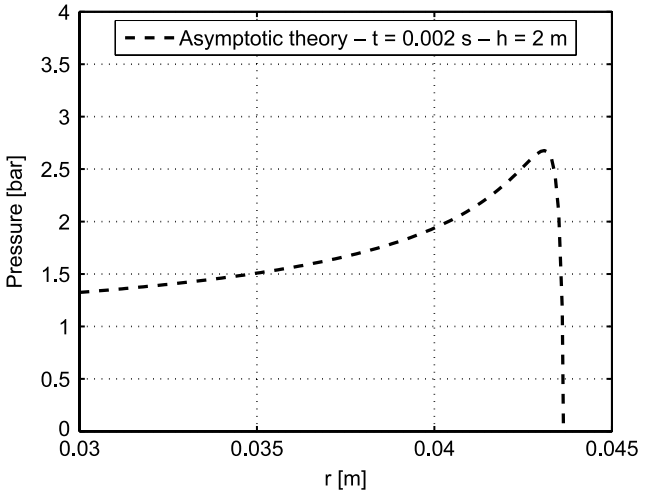

Fig. 4. Theoretical pressure distribution as a function of r for a cone with deadrise angle 20° and drop height 2 m.

pressure peaks occur in a very small time interval (order of magnitude milliseconds). For the same reason the resonance frequency of the sensors should be high enough. A small pressure cell diaphragm area is necessary since the pressure peaks are also very much localized in space as well, as can be seen in Fig. 4, showing the theoretically predicted pressure distribution according to asymptotic theory at $t = 0.002$ s for a cone with deadrise angle 20° and drop height 2 m.

Table 3
Influence of pressure sensor diameter: estimated deviations from peak pressure for drop heights of 1 m and 4 m.

Sensor diameter (mm)	$h = 1$ m (%)	$h = 4$ m (%)
5.5	10.8	13.9
19	30.5	34.2

In earlier investigations, sensors with larger diameters have sometimes been used, with values up to 19 mm in [16]. In that case the pressure peaks might have a smaller spatial extent than the sensor area. Even pressure cells with diameter 5.5 mm might measure a space-averaged pressure, which is slightly different from the peak pressure. The pressure distribution is particularly more peaked when the (local) deadrise angle is small and the impact velocity high. Assuming that a pressure cell registers the space-averaged pressure when subject to a non-uniform pressure distribution, the deviation between the peak pressure and the sensor record can be determined. In [23], Faltinsen estimated that the theoretical peak pressure is at maximum 11% higher than the space-averaged pressure, measured by a sensor with a diameter of 4 mm. Deviations of the same magnitude can be derived, based on the theoretically predicted pressure distribution by the three-dimensional asymptotic theory. For pressure cells with diameter 5.5 mm it is estimated with the latter method that the measured pressure on a cone with deadrise angle 20° deviates between 10% and 14% from the peak pressure for drop heights of 1 m and 4 m. In a similar way as above, it is expected that a pressure sensor with a diameter of 19 mm, would underestimate the peak pressure with more than 30% for the same case of a cone with deadrise angle 20°, as shown in Table 3.

2.2.2. High speed camera

A high speed camera was used to record the penetration of the impacting bodies as a function of time. The camera provided information on the water uprise along the body and on the position and velocity of the impacting body. For this purpose a marker tracking technique has been applied. The high speed camera is able to deliver images up to 250 000 frames per second (fps) and has full mega pixel resolution at 3000 fps. In this test case, it has been used at 5000 up to 18 000 fps, dependent on the desired pixel resolution. Because of the high frame rate, the camera shutter time is extremely short. In order to overcome low illumination and to avoid interference with the grid frequency, special flicker free lights have been used. Two lasers are mounted on top of the basin and serve as a trigger for the data acquisition system. When the dropped objects intersect the laser beams, the recording of the pressure sensors, accelerometer and camera signal starts automatically.

3. Analytical formulation

The experimental results are compared with existing asymptotic solutions based on the classical Wagner method extended to axisymmetric bodies, as it was proposed by Chuang [6] and Faltinsen et al. [7]. Despite the interesting work that has already been carried out in the field of water impact, Wagner's method is even nowadays still very valuable, since it produces analytical formulas that are easy to handle and give a very good first insight into the problem. The fluid flow is described by potential theory and a constant entry velocity U is assumed. The initial time instant t_0 is defined as the time where the body touches the calm water surface. At a time t, the penetration depth relative to the calm water surface ($z = 0$) equals Ut and the corresponding instantaneous radius at the wet section of the cone is $b_0(t)$, as shown in Fig. 5. The instantaneous radius $b(t)$ at the intersection point between the body and the water is found by integrating the vertical velocity of the water particles at $z = 0$. For a cone shape this results in $b(t) = 4Ut/(\pi \tan\beta)$ [7]. It should be mentioned that Fig. 5 gives a simplified presentation of the water uprise, since in reality a jet flow occurs which might end in a spray, depending on the convexity of the object.

The pressure on a cone shape with deadrise angle β, at a certain distance r from the symmetry axis, is expressed by:

$$p_{cone} = \frac{1}{2}\rho U^2 \left[1 - \frac{4\left(\frac{r}{Ut}\right)^2}{\pi^2\left(\frac{16}{\pi^2\tan^2\beta} - \left(\frac{r}{Ut}\right)^2\right)} + \frac{64}{\pi^3\tan^2\beta\sqrt{\frac{16}{\pi^2\tan^2\beta} - \left(\frac{r}{Ut}\right)^2}} \right]. \quad (1)$$

Eq. (1) is composed of three terms. The first term expresses the stagnation pressure. The second term is a consequence of the permanent flow around the disc and the third term accounts for the expansion of the disc, representing the effect of the non-stationary behaviour of the flow around the disc. As mentioned before, the blunt body assumption in Wagner's method implies that bodies should have small local deadrise angles. In the literature, it is stated that the classical Wagner theory gives quite accurate results for wedges with deadrise angles in the range of 4 to 20 degrees [13]. When deadrise angles are smaller than 4 degrees, an air cushion is formed, which reduces the pressure on the structure and as a result, Wagner theory overestimates the pressure by a large margin.

For a hemisphere the relationship between the penetration depth and instant wet radius b is not as straightforward as it is for a cone shape. Faltinsen and Zhao [7] suggested a quadratic relation between Ut and b which is only valid for small submergences

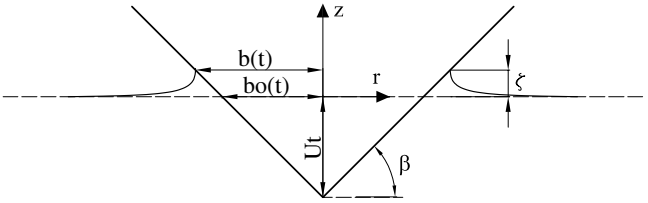

Fig. 5. Cone penetrating through originally calm water: clarification of parameters.

$(Ut/R < 1/5)$: $b = \sqrt{3RUt}$. The pressure on an impacting hemisphere with radius R, at a distance r from the symmetry axis, is expressed as follows:

$$p_{hemisphere} = \frac{1}{2}\rho U^2 \left[1 - \frac{4\left(\frac{r}{Ut}\right)^2}{\pi^2\left(\frac{3R}{Ut} - \left(\frac{r}{Ut}\right)^2\right)} + \frac{6}{\pi\sqrt{\frac{3Ut}{R} - \left(\frac{r}{R}\right)^2}} \right]. \quad (2)$$

The measured penetration and acceleration will be compared with theoretical values that are based on the computation of the hydrodynamic impact force, F_3, acting on a body penetrating the free water surface. This force is calculated in two ways. By making use of the added mass theorem (AM), F_3 can be expressed as:

$$F_3 = \frac{\mathrm{d}\left(M_{a_{33}}U\right)}{\mathrm{d}t} = M_{a_{33}}\frac{\mathrm{d}^2z}{\mathrm{d}t^2} + \frac{\mathrm{d}M_{a_{33}}}{\mathrm{d}t}\frac{\mathrm{d}z}{\mathrm{d}t} \quad (3)$$

where $M_{a_{33}}$ is the high frequency limit of the added mass. The second term in Eq. (3) can also be computed by integration of the pressures given in Eqs. (1) and (2). This will be referred to as the pressure integration (PI) method. When F_3 is known, the acceleration at each time step is derived and the velocity and penetration depth are obtained by numerical integration of the acceleration.

4. Experimental test results

4.1. Water uprise and impact velocity

Fig. 6 shows a selected number of images of a hemisphere penetrating the free water surface, dropped from 1 m. A software program recognizes the pattern of the marker and determines its coordinates at each time step. Consequently the position of the body is known as a function of time and the velocity can be determined. The pictures clearly show the water uprise along the hemisphere. The jet flow is quickly detached from the body surface ending up in a spray. This phenomenon has also been observed for cylinders by Greenhow and Lin in [28] and [29]. Figs. 7 and 8 show camera images of the impacting cones for a drop height of 1 m. The creation and propagation of a jet along the cone surface can be clearly seen and measured.

From the photographs of the cones the ratio C_w can be determined and compared with theoretical values. The C_w factor is defined as the ratio between the heights of the immediate and undisturbed free water surfaces measured from the bottom point of the falling object:

$$C_w = 1 + \frac{\zeta(b,t)}{Ut} \quad (4)$$

with ζ the z-coordinate of the intersection point between the object and the free water surface, see Fig. 5. When flow separation occurs above ζ, as in the case of the hemisphere, C_w has the physical meaning of a wetting factor. However, in the case of a cone a thin jet flow might occur above this intersection point as observed in Figs. 7 and 8. The wetting factor C_w for a cone with attached jet flow can then be defined as:

$$C_w = 1 + \frac{\zeta(b,t) + l_{jet}}{Ut} = \frac{b}{b_0} + \frac{l_{jet}}{Ut} \quad (5)$$

where l_{jet} is the height of the jet. Considering the outer flow

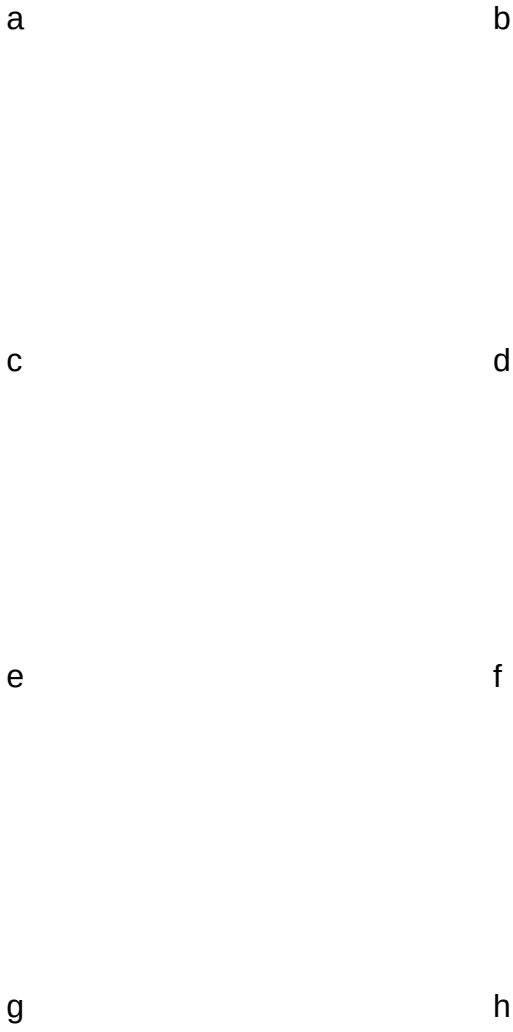

Fig. 6. Hemisphere penetrating the water – (a) $t = 0.0000$ s, (b) $t = 0.0022$ s, (c) $t = 0.0044$ s, (d) $t = 0.0066$ s, (e) $t = 0.0088$ s, (f) $t = 0.0110$ s, (g) $t = 0.0132$ s.

Fig. 7. Cone ($\beta = 20^\circ$) penetrating the water – (a) $t = 0.0000$ s, (b) $t = 0.0044$ s, (c) $t = 0.0088$ s, (d) $t = 0.0132$ s.